

**Fast and Stable Li Metal Anode Enabled by Mo<sub>6</sub>S<sub>8</sub> Artificial Interphase with Super Li-ion Conductivity**

Journal:	<i>Journal of Materials Chemistry A</i>
Manuscript ID	TA-ART-12-2018-012450.R1
Article Type:	Paper
Date Submitted by the Author:	04-Feb-2019
Complete List of Authors:	Lu, Ke; Northern Illinois University, Chemistry Gao, Siyuan; Northern Illinois University, Chemistry Dick, Robert; Trine University Sattar, Zain; Northern Illinois University, Chemistry Cheng, Yingwen; Northern Illinois University College of Liberal Arts and Sciences, Chemistry and Biochemistry

# **Fast and Stable Li Metal Anode Enabled by Mo<sub>6</sub>S<sub>8</sub> Artificial Interphase with Super Li-ion Conductivity**

Ke Lu <sup>a</sup>, Siyuan Gao <sup>a</sup>, Robert J. Dick <sup>b</sup>, Zain Sattar <sup>a</sup> and Yingwen Cheng <sup>a,\*</sup>

<sup>a</sup> Department of Chemistry and Biochemistry, Northern Illinois University, DeKalb, IL 60115, United States

<sup>b</sup> Department of Science, Trine University, Angola, IN 46703, United States

\*E-mail: [ycheng@niu.edu](mailto:ycheng@niu.edu)

**Abstract**

The poor interfacial stability of Li metal leads to formation of unstable solid-electrolyte interphases (SEI) and severely limits its practical applications. Protecting Li metal with artificial SEI that has balanced properties between stability, conductivity and mechanical strength is critical. Here we demonstrate a design strategy of stabilizing Li using Mo<sub>6</sub>S<sub>8</sub>/carbon artificial SEI films. These films are directly coated on Li foils and the Mo<sub>6</sub>S<sub>8</sub> particles provide ordered conduction channels for fast but regulated Li-ion flux, and enabled hybrid anodes that have nearly four times higher exchange current densities. They also have seamless contact with Li metal and protect it from parasitic reactions, and hence significantly improve its stability. Consequently, Li metal batteries in which the hybrid anodes were paired with LiNi<sub>0.8</sub>Mn<sub>0.1</sub>Co<sub>0.1</sub>O<sub>2</sub> cathodes (3.0 mAh per cell) exhibited significantly improved cyclic stability (63% vs 25% retention) and stabilized Li interphase compared with pristine Li anodes.

**Keywords:** Artificial SEI, Li metal, Li protection, Ni-rich cathodes

Li metal is commonly considered as the ultimate anode material for high energy density batteries because of its unique properties particularly the highest theoretical capacity of  $3860 \text{ mAh g}^{-1}$ , low density of  $0.59 \text{ g cm}^{-3}$ , and the lowest electrochemical potential ( $-3.040 \text{ V}$  vs. standard hydrogen electrode).<sup>1-3</sup> Unfortunately, Li metal has extremely high reactivity with almost all battery electrolytes and produce solid-electrolyte interphases (SEI) that are unstable, nonuniform and have low Li-ion conductivity. The formation of SEI causes irreversible loss of battery materials and fluctuations in local current densities and Li ion concentrations,<sup>4-6</sup> which results in substantial polarization increases and Li corrosion along with dendrite growth during Li plating and stripping.<sup>7</sup> Consequently, current Li anode suffer severely from low coulombic efficiency and poor cycling stability, especially in the carbonate-based electrolytes that are compatible with the current 4V intercalation cathodes.<sup>8-9</sup>

Modifying SEI properties with artificial protection layers recently appeared as an attractive approach to address the instability issue.<sup>10</sup> The composition and structure of these layers, in principle, could be tuned precisely to allow seamless contact with Li metal and provide simultaneously improved interfacial stability and balanced electronic/ionic conductivity that are required for stable battery cycling. Artificial SEI films composed of LiF,<sup>11-12</sup> Li-metal alloys,<sup>13-15</sup> nitrides,<sup>16</sup> cross-linked polymers,<sup>8</sup>  $\text{Li}_3\text{PS}_4$ ,<sup>17</sup>  $\text{Li}_3\text{PO}_4$ ,<sup>18</sup> have been described. Notably, these are usually ultrathin films that were coated on Li metal through separate in-situ reactions by immersing Li in a liquid solution that contains reactive precursors.<sup>13-14, 19-21</sup> These coatings have been shown effective to suppress side-reactions and dendrite growth, particularly under low

current conditions and at the initial stages of cycling. However, they usually have limited Li-ion conductivity and/or poor flexibility, and could crack during cycling. Overall, it is still very challenging to design SEI films that could be directly coated on Li metal and afford their stable operation.<sup>22</sup>

Herein, we describe a new strategy of designing transferrable artificial SEI layers and demonstrate their remarkable capability for providing substantially improved interphasical stability to Li metal (Fig. 1a). These artificial layers was based on the Chevrel phase Mo<sub>6</sub>S<sub>8</sub>/carbon composites, which are known for superior ionic conductivity and outstanding stability.<sup>23-24</sup> We hypothesized that artificial layers designed with robust materials that have rapid Li-ions diffusion could effectively protect Li metal from side-reactions without sacrificing the stripping/plating kinetics, and the use of transferrable films allows for precise thickness and composition control and facilitates scalable production of hybrid anodes.<sup>22</sup> We discovered that the protected hybrid anodes have substantially increased Li-ions transport kinetics along with outstanding surface stability under aggressive cycling conditions. As a result of the stabilized Li surface without parasitic reactions, prototype Li metal batteries employing high loading LiNi<sub>0.8</sub>Mn<sub>0.1</sub>Co<sub>0.1</sub>O<sub>2</sub> (NMC-811) cathodes exhibited drastically enhanced cycling stability in a carbonate electrolyte compared with unmodified Li anodes.

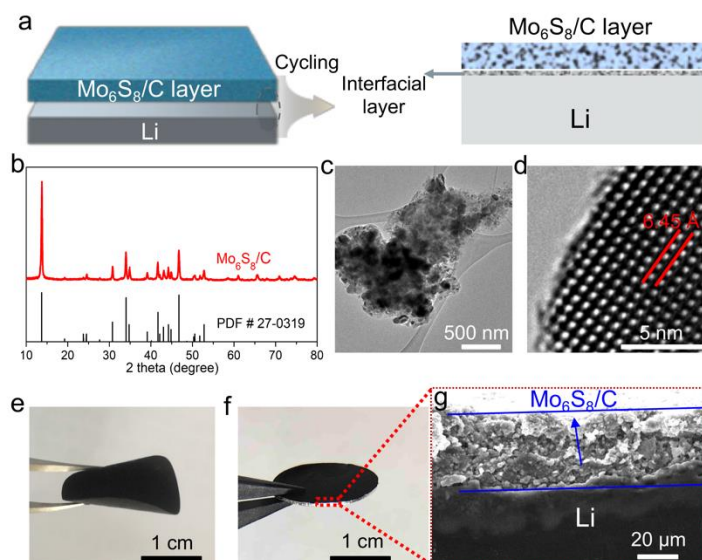


Figure 1: a) Schematic illustrations of protecting Li metal with  $\text{Mo}_6\text{S}_8/\text{C}$  artificial SEI layers and b-g) structural characterizations of  $\text{Mo}_6\text{S}_8$  particles and the hybrid anodes: b) X-ray diffraction pattern and c-d) TEM images of  $\text{Mo}_6\text{S}_8/\text{C}$  composite; photographs of e) a piece of  $\text{Mo}_6\text{S}_8/\text{C}$  thin film and f) protected hybrid Li metal anode; g) SEM image of the interphase between  $\text{Mo}_6\text{S}_8/\text{C}$  layer and Li metal that shows their intimate contact without separation.

The Chevrel phase  $\text{Mo}_6\text{S}_8/\text{carbon}$  composites were obtained by acid leaching of  $\text{Cu}^{2+}$  off  $\text{Cu}_2\text{Mo}_6\text{S}_8/\text{carbon}$ , which were synthesized from precursors including 0.6 g carbon, 3.0 g  $\text{MoS}_2$ , 1.8 g Mo and 1.2 g CuS. These precursors were first ball-milled and then calcinated under Ar at  $1000^\circ\text{C}$  for 10 hrs (detailed in Supplemental Information). Pristine  $\text{Mo}_6\text{S}_8$  particles without carbon were also synthesized for comparison. It should be noted that this method is more scalable, faster and requires less work for producing high quality Chevrel phase compounds compared with typical methods.<sup>25-27</sup> The combined XRD and TEM characterizations confirmed nearly 100% production of  $\text{Mo}_6\text{S}_8$  both for the synthesis with (Fig. 1b-c) and without (Fig. S1-2) carbon but particles synthesized with carbon have smaller size and better conductivity, which are beneficial for faster ion transport necessary for improving battery operations.<sup>26</sup>  $\text{Mo}_6\text{S}_8$  has inherent large open channels ( $\sim 6.45 \text{ \AA}$ , Fig. 1d) between

nearby clusters, which are ideal for stable and fast diffusion of a variety of cations.<sup>23</sup>

<sup>26</sup> When used as hosts for insertion of  $\text{Li}^+$ , they delivered a specific capacity of 112 mAh/g at 0.1C and retained ~ 66% of the this capacity when the rate was increased to 20 C in the voltage range of 1.5~2.9V, along with superior stability (Fig. S3).

Thin films composed of  $\text{Mo}_6\text{S}_8/\text{C}$  or  $\text{Mo}_6\text{S}_8$  particles were prepared using polytetrafluoroethylene (PTFE) as the binder. These films (Fig. 1e) had thicknesses of ~40  $\mu\text{m}$  and areal densities of ~ 3.5  $\text{mg cm}^{-2}$ , and they were pressed onto the surface of bulk Li anodes (450  $\mu\text{m}$  thickness) at 500 psi using a hydraulics press (Fig. 1f). The SEM image reveals that the  $\text{Mo}_6\text{S}_8$  film and Li metal had seamless intimate contact without separation (Fig. 1g). These hybrid anodes were first assembled into coin cells using 1.0M  $\text{LiPF}_6$  in EC/DEC for evaluation of Li ions transport properties and interfacial stabilities. The direct contact of  $\text{Mo}_6\text{S}_8$  with Li metal in the presence of electrolyte leads to rapid Li-ions diffusion to the  $\text{Mo}_6\text{S}_8$  framework, in a way similar as battery short-circuit, and results in formation of Li-ion conductive lithiated  $\text{Li}_x\text{Mo}_6\text{S}_8$ . The value of x was estimated as 16 using the capacity of discharging the  $\text{Li}||\text{Mo}_6\text{S}_8$  cells to 0.0V (Fig. S4). The exact structure of the fully discharged product  $\text{Li}_{16}\text{Mo}_6\text{S}_8$  is complex but XRD analysis suggests dominance of the Chevrel phase crystal structure (Fig. S5). The hybrid anodes were therefore function as  $\text{Li}_{16}\text{Mo}_6\text{S}_8$  coated Li metal. We reason that the  $\text{Li}_{16}\text{Mo}_6\text{S}_8$  layer has better interfacial stability compared with pristine Li and provides three-dimensional channels for fast but regulate Li-ion flux that regulate Li stripping and plating, which is critical for mitigating formation of dendritic structures and improving SEI stability (Fig. 1a).

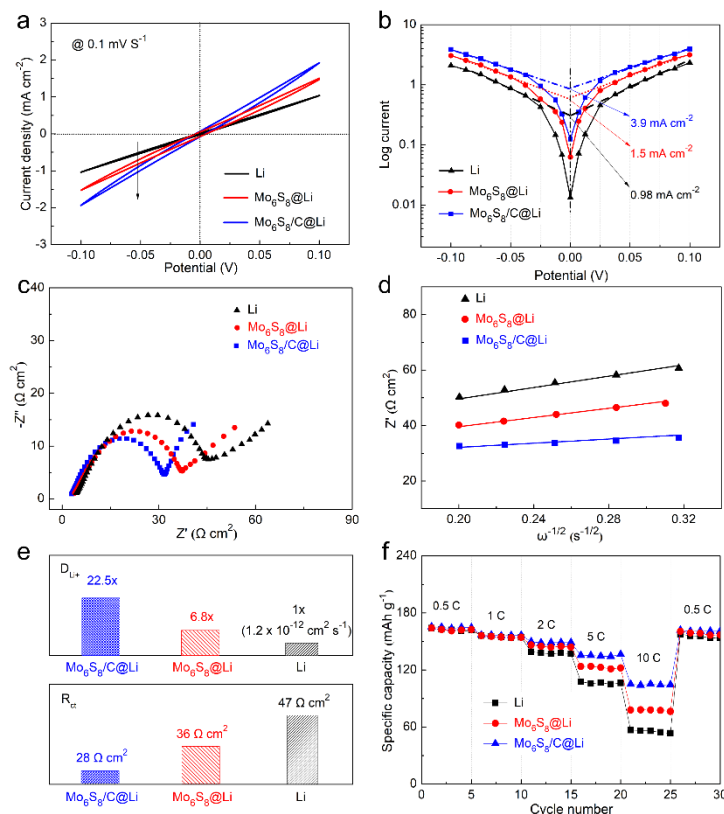


Figure 2:  $\text{Mo}_6\text{S}_8/\text{C}@\text{Li}$  hybrid anodes have enhanced Li-ion transfer kinetics: a) cyclic voltammogram ( $0.1 \text{ mV s}^{-1}$ ) for symmetric cells assembled with pristine or hybrid anodes; b) Tafel plots obtained from analyzing results shown in a); c) Nyquist plots acquired from the symmetric cells and d-e) analysis of EIS results for Li-ion diffusion coefficient and charge-transfer resistance; f) rate capability of prototype full cells in which the different Li anodes are paired with NMC-811 cathode.

The Li ions plating/stripping properties of the hybrid Li anodes were evaluated using symmetric coin cells. Fig. 2a compares the cyclic voltammograms (CV) of different anodes acquired at  $0.1 \text{ mV s}^{-1}$  with a voltage range of  $-0.1$  to  $0.1 \text{ V}$ . They all exhibited linear shaped and symmetric polarization curves, suggesting dominance of  $\text{Li}/\text{Li}^+$  redox couple without obvious side redox reactions.<sup>28</sup> Importantly, both of the hybrid anodes exhibited steeper slopes that corresponding to faster Li deposition/stripping kinetics compared with pristine Li anodes. The analysis of these results using the Tafel relationship yields their exchange current densities (Fig. 3b). The  $\text{Mo}_6\text{S}_8/\text{C}@\text{Li}$  anode had the best Li-ion charge transfer kinetics, evidenced with

substantially higher exchange current of  $3.9 \text{ mA cm}^{-2}$  compared with the  $\text{Mo}_6\text{S}_8@\text{Li}$  ( $1.5 \text{ mA cm}^{-2}$ ) and pristine Li ( $0.98 \text{ mA cm}^{-2}$ ) anodes.

The symmetric cells were also examined using electrochemical impedance spectroscopy (EIS) at open circuit potential and the obtained Nyquist plots are shown in Fig. 2c. These spectra were analyzed using the equivalent circuit model shown in Fig. S6 for estimation of charge-transfer resistance ( $R_{ct}$ ), Warburg impedance ( $Z_w$ ) and Li-ions diffusion coefficient ( $D_{\text{Li}^+}$ ). The  $\text{Mo}_6\text{S}_8/\text{C}@\text{Li}$  anode outperformed both  $\text{Mo}_6\text{S}_8@\text{Li}$  and pristine Li anodes, and exhibited the lowest charge transfer resistance of only  $28 \Omega \text{ cm}^2$  and the highest  $\text{Li}^+$  diffusion coefficient that reached  $2.7 \times 10^{-11} \text{ cm}^2 \text{ s}^{-1}$  (Fig. 2e). The improved kinetics with the hybrid anodes also ensured Li metal batteries with much better rate performance. Specifically, the different Li anodes were paired with the intercalation cathode  $\text{LiNi}_{0.8}\text{Mn}_{0.1}\text{Co}_{0.1}\text{O}_2$  (NMC-811, coated on Al foils at  $9.12 \text{ mg cm}^{-2}$ ). The cathodes were punched to relatively large discs ( $16 \text{ mm}$ ,  $2.0 \text{ cm}^2$ ) and each disc deliver a capacity of  $\sim 3 \text{ mAh}$  at 1C. The rate test shows that the  $\text{Mo}_6\text{S}_8/\text{C}@\text{Li}$  hybrid anode afford full cells with the best high rate performance (Fig. 2f), with 48% capacity retention the rate was increased to from 0.1 to 10 C. In comparison, the  $\text{Li}||\text{NMC-811}$  battery only had 35% retention. These results reinforce the conclusions drawn from the CV and EIS results on that the  $\text{Mo}_6\text{S}_8/\text{C}$  artificial SEI layer promoted faster Li-ion transfer even though these films are relatively thick compared with typical SEI layers reported in the literature,<sup>29-31</sup> perhaps due to the inherent fast cation transport kinetics of the Chevrel phase compounds and/or the increased electrochemical active surface area with the introduction of  $\text{Mo}_6\text{S}_8/\text{C}$

nanoparticles.

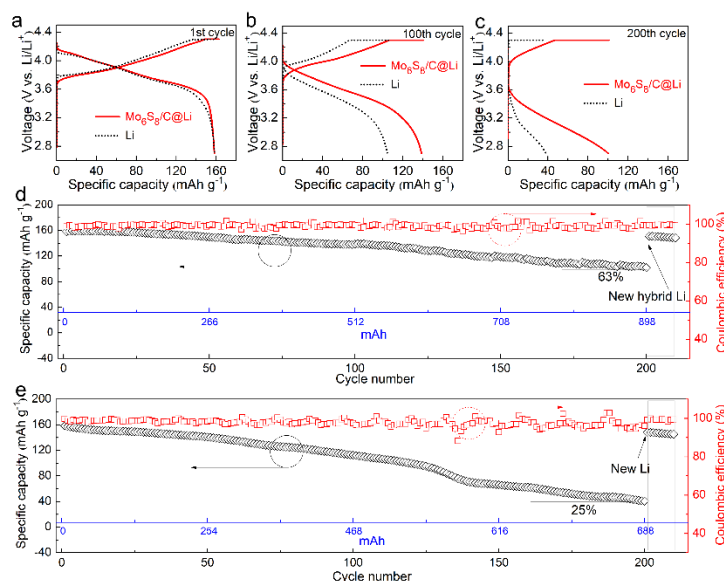


Figure 3. Mo<sub>6</sub>S<sub>8</sub>/C@Li hybrid anodes significantly improved the cycling stability of Li metal batteries paired with the NMC-811 cathodes: comparison of voltage profiles at a) the first; b) 100<sup>th</sup>; and c) 200<sup>th</sup> cycles; and cycling stability of full cells assembled with e) hybrid Li anodes and f) pristine Li anodes at 1.0 C (1.52 mA cm<sup>-2</sup>).

The artificial SEI layers based on Mo<sub>6</sub>S<sub>8</sub>/C significantly improved the cyclic stability of Li metal both under symmetric cell and full cell configurations. The symmetric cell with hybrid anodes only had slight polarization increases (to 0.17V) after 600 hrs of cycling at 1.0 mA cm<sup>-2</sup> for 1.0 mAh cm<sup>-2</sup> per cycle (Fig. S7), which is much smaller than pristine Li anodes. The Li metal full cells were assembled with the same high-loading NMC-811 cathode and tested under 2.7 ~ 4.3 V for 200 cycles (Fig. 3). The NMC-811 is one of the most promising cathode materials but is very challenging to work together with Li metal due to its reactivity with electrolytes that form corrosive intermediates to degrade Li metal.<sup>32-33</sup> The batteries were cycled at a current of 3.04 mA (equivalent of 1.52 mA cm<sup>-2</sup>, 1C rate), which is usually considered as aggressive currents because the degradation of Li metal is accelerated.<sup>34</sup> The battery with a hybrid anode delivered similar initial capacities as the one with pristine

Li metal (at  $\sim 160 \text{ mAh g}^{-1}$ ) and their voltage profiles are nearly identical (Fig. 3a), indicating the artificial SEI layers didn't affect the behavior of Li anode which agree with observations from Fig. 2a. The capacity of both batteries decreased slowly during the first 100 cycles (Fig. 3 d-e), and the hybrid anode afforded smaller polarization increase and notably better stability, with a capacity retention of 88% as compared with 71% for pristine Li anode battery (Fig. 3b).

As the cycling continues a typical rapid capacity decay at  $\sim 120$  cycles was observed for the battery with pristine Li anode due to nearly complete degradation of Li metal as previously described.<sup>34-35</sup> The Columbic efficiency (CE) also dropped to  $\sim 92\%$  and the overall retention was only 25% (Fig. 3c). In contrast, the battery with the hybrid anode maintained highly efficient cycling (99.6% average CE) and had much better stability without abnormal decay, and overall retained 63% of the initial capacity after 200 cycles. Fig. 3d-e also compared the total capacity cycled through Li anodes (blue colored X-axis). The hybrid anodes had superior stability and sustained a total capacity of 898 mAh, which is among the best for Li metal protection under similar conditions.<sup>8</sup> In addition, it should be noted that the observed capacity decay originate mostly from the anode, as cells re-assembled with the same cathode but with fresh anodes and electrolytes recovered the initial capacities (Fig.3). Furthermore, the impedance of these batteries was also collected during cycling (Fig. 4 a-b). The  $R_{ct}$  was analyzed using the equivalent circuit model outlined in Fig. S8 and the results are included in the insets. Notably, the cell equipped with the hybrid anode had much better stability, and the  $R_{ct}$  increased from the initial 45 to  $165 \Omega \text{ cm}^2$  after the 200

cycles. In strong contrast, the pristine Li anode reached to a much higher resistance of 425  $\Omega \text{ cm}^2$  after the same testing.

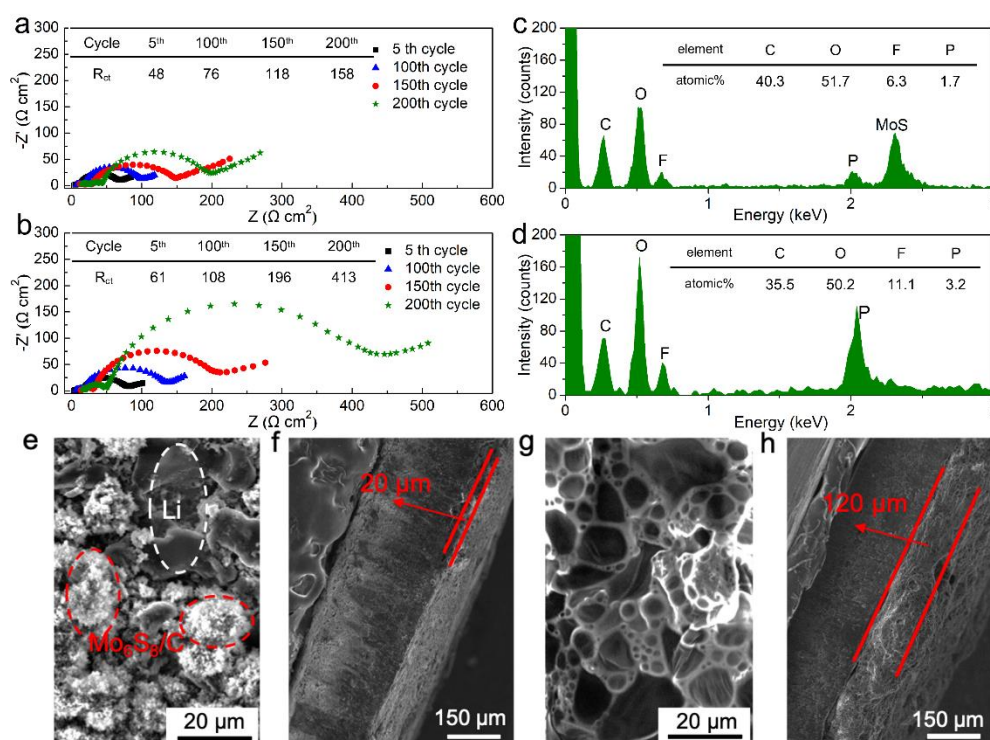


Figure 4:  $\text{Mo}_6\text{S}_8/\text{C}$  artificial layers stabilize Li metal in carbonate electrolytes: Nyquist plot acquired at different stage of cycling for Li metal batteries with a) hybrid anode and b) pristine Li anode; post-mortem c-d) EDS spectra and e-h) SEM images of the c,e,f) hybrid anode and d,g,h) pristine Li anode after 200 cycles with the NMC-811 cathodes.

The effective protection of Li metal with artificial SEI layers was further confirmed with post-mortem analysis of Li anodes with EDS and SEM (Fig. 4, S9-10). After 200 cycles, the SEI generated in the protected Li anode was much thinner (only  $\sim 20 \mu\text{m}$ ) and the detected F and P concentrations were only half of the pristine Li anode (Fig. 4c-d). The surface of protected Li was also much smoother without obvious dendritic or mossy structures, whereas the pristine Li anode had rather thick ( $\sim 120 \mu\text{m}$ ) SEI that appeared extremely porous (Fig. 4e-h, and S9-10 for additional SEM images). Notably, no Li growth was observed on the surface or within the bulk of the  $\text{Mo}_6\text{S}_8/\text{C}$  artificial SEI layers, suggesting the presence of  $\text{Mo}_6\text{S}_8$  didn't affect

the growth behavior of Li metal. This is supported by the fact that the Li nucleation overpotential on lithiated  $\text{Mo}_6\text{S}_8$  was rather high ( $\sim 89$  mV at  $2 \text{ mA cm}^{-2}$ ) as shown in Figure S11<sup>11,15</sup>. In addition, the artificial SEI layer maintained intimate contact with the metallic Li during battery cycling, as no segregation or peeling off was observed after the 200 cycles (Figure S12). These combined electrochemical and post-mortem analysis therefore further strengthened the exceptional capability of the artificial SEI layers proposed in this work on isolation of Li and effectively mitigate its side-reactions with electrolyte, and provided significantly improved interfacial stability.

In conclusion, we describe the design of transferrable artificial SEI layers using  $\text{Mo}_6\text{S}_8/\text{C}$  particles to improve the practical stability of Li metal in carbonate electrolytes. We discovered that Li anodes coated with  $\text{Mo}_6\text{S}_8/\text{C}$  films have substantially increased exchange current densities that could attribute to the promoted and regulated Li-ion flux through the lithiated  $\text{Mo}_6\text{S}_8$  frameworks. The  $\text{Li}_{16}\text{Mo}_6\text{S}_8/\text{C}$  films have intimate interaction with Li metal and protect it from parasitic reactions, which result in hybrid Li anodes that have stabilized interphases for practical applications as demonstrated with significantly improved cyclic stability for prototype full cells coupled with high-loading NMC-811 cathodes.

### **Supplemental Information**

Complete experimental details and additional characterizations results, including supplemental Figures S1-S12.

### **Acknowledgements**

This work was supported by startup funds provided to Y. C. from Northern Illinois University. R. D. acknowledges the support from the U.S. National Science

Foundation REU program, under Award CHE-1659548. Z. S. was a summer research volunteer from Bartlett High School in Bartlett, IL 60103. The NMC cathodes were produced at the U.S. Department of Energy's (DOE) CAMP (Cell Analysis, Modeling and Prototyping) Facility, Argonne National Laboratory. The CAMP Facility is fully supported by the DOE Vehicle Technologies Program (VTP) within the core funding of the Applied Battery Research (ABR) for Transportation Program.

## References

1. Cheng, X.-B.; Zhang, R.; Zhao, C.-Z.; Zhang, Q., Toward Safe Lithium Metal Anode in Rechargeable Batteries: A Review. *Chemical Reviews* **2017**, *117* (15), 10403-10473.
2. Albertus, P.; Babinec, S.; Litzelman, S.; Newman, A., Status and challenges in enabling the lithium metal electrode for high-energy and low-cost rechargeable batteries. *Nature Energy* **2018**, *3* (1), 16-21.
3. Lu, K.; Zhang, H.; Gao, S.; Ma, H.; Chen, J.; Cheng, Y., Manipulating Polysulfide Conversion with Strongly Coupled Fe<sub>3</sub>O<sub>4</sub> and Nitrogen Doped Carbon for Stable and High Capacity Lithium–Sulfur Batteries. *Advanced Functional Materials* **2018**, *0* (0), 1807309.
4. Vaughey, J. T.; Liu, G.; Zhang, J.-G., Stabilizing the surface of lithium metal. *MRS Bulletin* **2014**, *39* (05), 429-435.
5. Aurbach, D.; Zinigrad, E.; Cohen, Y.; Teller, H., A short review of failure mechanisms of lithium metal and lithiated graphite anodes in liquid electrolyte solutions. *Solid State Ionics* **2002**, *148* (3), 405-416.
6. Wu, B.; Wang, S.; Lochala, J.; Desrochers, D.; Liu, B.; Zhang, W.; Yang, J.; Xiao, J., The role of the solid electrolyte interphase layer in preventing Li dendrite growth in solid-state batteries. *Energy & Environmental Science* **2018**, *11* (7), 1803-1810.
7. Verma, P.; Maire, P.; Novák, P., A review of the features and analyses of the solid electrolyte interphase in Li-ion batteries. *Electrochimica Acta* **2010**, *55* (22), 6332-6341.
8. Gao, Y.; Zhao, Y.; Li, Y. C.; Huang, Q.; Mallouk, T. E.; Wang, D., Interfacial Chemistry Regulation via a Skin-Grafting Strategy Enables High-Performance Lithium-Metal Batteries. *J Am Chem Soc* **2017**, *139* (43), 15288-15291.
9. Xu, W.; Wang, J.; Ding, F.; Chen, X.; Nasybulin, E.; Zhang, Y.; Zhang, J.-G., Lithium metal anodes for rechargeable batteries. *Energy & Environmental Science* **2014**, *7* (2), 513-537.
10. Cha, E.; Patel, M. D.; Park, J.; Hwang, J.; Prasad, V.; Cho, K.; Choi, W., 2D MoS<sub>2</sub> as an efficient protective layer for lithium metal anodes in high-performance Li–S batteries. *Nature Nanotechnology* **2018**, *13* (4), 337-344.
11. Zhao, J.; Liao, L.; Shi, F.; Lei, T.; Chen, G.; Pei, A.; Sun, J.; Yan, K.; Zhou, G.; Xie, J.; Liu, C.; Li, Y.; Liang, Z.; Bao, Z.; Cui, Y., Surface Fluorination of Reactive Battery Anode Materials for Enhanced Stability. *J Am Chem Soc* **2017**, *139* (33), 11550-11558.
12. Xu, R.; Zhang, X.-Q.; Cheng, X.-B.; Peng, H.-J.; Zhao, C.-Z.; Yan, C.; Huang, J.-Q., Artificial Soft-Rigid Protective Layer for Dendrite-Free Lithium Metal Anode. *Advanced Functional Materials* **2018**, *28* (8).
13. Pang, Q.; Liang, X.; Kochetkov, I. R.; Hartmann, P.; Nazar, L. F., Stabilizing Lithium Plating by a Biphasic Surface Layer Formed In Situ. *Angew Chem Int Ed Engl* **2018**, *57* (31), 9795-9798.
14. Liang, X.; Pang, Q.; Kochetkov, I. R.; Sempere, M. S.; Huang, H.; Sun, X.; Nazar, L. F., A facile surface chemistry route to a stabilized lithium metal anode. *Nature Energy* **2017**, *2* (9).

15. Tu, Z.; Choudhury, S.; Zachman, M. J.; Wei, S.; Zhang, K.; Kourkoutis, L. F.; Archer, L. A., Fast ion transport at solid–solid interfaces in hybrid battery anodes. *Nature Energy* **2018**, *3* (4), 310-316.
16. Liu, Y.; Lin, D.; Yuen, P. Y.; Liu, K.; Xie, J.; Dauskardt, R. H.; Cui, Y., An Artificial Solid Electrolyte Interphase with High Li-Ion Conductivity, Mechanical Strength, and Flexibility for Stable Lithium Metal Anodes. *Adv Mater* **2017**, *29* (10).
17. Liang, J.; Li, X.; Zhao, Y.; Goncharova, L. V.; Wang, G.; Adair, K. R.; Wang, C.; Li, R.; Zhu, Y.; Qian, Y.; Zhang, L.; Yang, R.; Lu, S.; Sun, X., In Situ Li<sub>3</sub>PS<sub>4</sub> Solid-State Electrolyte Protection Layers for Superior Long-Life and High-Rate Lithium-Metal Anodes. *Adv Mater* **2018**, e1804684.
18. Li, N. W.; Yin, Y. X.; Yang, C. P.; Guo, Y. G., An Artificial Solid Electrolyte Interphase Layer for Stable Lithium Metal Anodes. *Adv Mater* **2016**, *28* (9), 1853-8.
19. Pang, Q.; Liang, X.; Shyamsunder, A.; Nazar, L. F., An In Vivo Formed Solid Electrolyte Surface Layer Enables Stable Plating of Li Metal. *Joule* **2017**, *1* (4), 871-886.
20. Trinh, N. D.; Lepage, D.; Ayme-Perrot, D.; Badia, A.; Dolle, M.; Rochefort, D., An Artificial Lithium Protective Layer that Enables the Use of Acetonitrile-Based Electrolytes in Lithium Metal Batteries. *Angew Chem Int Ed Engl* **2018**, *57* (18), 5072-5075.
21. Zhang, X.-Q.; Chen, X.; Cheng, X.-B.; Li, B.-Q.; Shen, X.; Yan, C.; Huang, J.-Q.; Zhang, Q., Highly Stable Lithium Metal Batteries Enabled by Regulating the Solvation of Lithium Ions in Nonaqueous Electrolytes. *Angewandte Chemie* **2018**, *130* (19), 5399-5403.
22. Kim, M. S.; Ryu, J.-H.; Deepika; Lim, Y. R.; Nah, I. W.; Lee, K.-R.; Archer, L. A.; Il Cho, W., Langmuir–Blodgett artificial solid-electrolyte interphases for practical lithium metal batteries. *Nature Energy* **2018**, *3* (10), 889-898.
23. Levi, E.; Gershinshy, G.; Aurbach, D.; Isnard, O.; Ceder, G., New Insight on the Unusually High Ionic Mobility in Chevrel Phases. *Chemistry of Materials* **2009**, *21* (7), 1390-1399.
24. Yue, J.; Zhu, X.; Han, F.; Fan, X.; Wang, L.; Yang, J.; Wang, C., A Long-Cycle Life All-Solid-State Sodium Ion Battery. *ACS Applied Materials & Interfaces* **2018**.
25. Saha, P.; Jampani, P. H.; Datta, M. K.; Hong, D.; Gattu, B.; Patel, P.; Kadakia, K. S.; Manivannan, A.; Kumta, P. N., A rapid solid-state synthesis of electrochemically active Chevrel phases (Mo<sub>6</sub>T<sub>8</sub>; T = S, Se) for rechargeable magnesium batteries. *Nano Research* **2017**, *10* (12), 4415-4435.
26. Cheng, Y.; Parent, L. R.; Shao, Y.; Wang, C.; Sprenkle, V. L.; Li, G.; Liu, J., Facile Synthesis of Chevrel Phase Nanocubes and Their Applications for Multivalent Energy Storage. *Chemistry of Materials* **2014**, *26* (17), 4904-4907.
27. Lancy, E.; Lancy, E.; Levi, E.; Levi, E.; Mitelman, A.; Mitelman, A.; Malovany, S.; Malovany, S.; Aurbach, D.; Aurbach, D., Molten salt synthesis (MSS) of Cu<sub>2</sub>Mo<sub>6</sub>S<sub>8</sub>—New way for large-scale production of Chevrel phases. *Journal of Solid State Chemistry* **2006**, *179* (6), 1879-1882.
28. Kozen, A. C.; Lin, C.-F.; Pearse, A. J.; Schroeder, M. A.; Han, X.; Hu, L.; Lee, S.-B.; Rubloff, G. W.; Noked, M., Next-Generation Lithium Metal Anode Engineering via Atomic Layer Deposition. *ACS Nano* **2015**, *9* (6), 5884-5892.
29. Wei, S.; Choudhury, S.; Tu, Z.; Zhang, K.; Archer, L. A., Electrochemical Interphases for High-Energy Storage Using Reactive Metal Anodes. *Accounts of Chemical Research* **2018**, *51* (1), 80-88.
30. Li, Y.; Sun, Y.; Pei, A.; Chen, K.; Vailionis, A.; Li, Y.; Zheng, G.; Sun, J.; Cui, Y., Robust Pinhole-free Li<sub>3</sub>N Solid Electrolyte Grown from Molten Lithium. *ACS Cent Sci* **2018**, *4* (1), 97-104.
31. Xin, S.; You, Y.; Wang, S.; Gao, H.-C.; Yin, Y.-X.; Guo, Y.-G., Solid-State Lithium Metal Batteries Promoted by Nanotechnology: Progress and Prospects. *ACS Energy Letters* **2017**, *2* (6), 1385-1394.

32. Li, M.; Lu, J.; Chen, Z.; Amine, K., 30 Years of Lithium-Ion Batteries. *Adv Mater* **2018**, e1800561.
33. Yu, Y.; Karayaylali, P.; Katayama, Y.; Giordano, L.; Gauthier, M.; Maglia, F.; Jung, R.; Lund, I.; Shao-Horn, Y., Coupled LiPF<sub>6</sub> Decomposition and Carbonate Dehydrogenation Enhanced by Highly Covalent Metal Oxides in High-Energy Li-Ion Batteries. *The Journal of Physical Chemistry C* **2018**.
34. Zheng, J.; Engelhard, M. H.; Mei, D.; Jiao, S.; Polzin, B. J.; Zhang, J.-G.; Xu, W., Electrolyte additive enabled fast charging and stable cycling lithium metal batteries. *Nature Energy* **2017**, *2*, 17012.
35. Lu, D.; Shao, Y.; Lozano, T.; Bennett, W. D.; Graff, G. L.; Polzin, B.; Zhang, J.; Engelhard, M. H.; Saenz, N. T.; Henderson, W. A.; Bhattacharya, P.; Liu, J.; Xiao, J., Failure Mechanism for Fast-Charged Lithium Metal Batteries with Liquid Electrolytes. *Advanced Energy Materials* **2014**, *5* (3), 1400993.

## TOC

